Ferromagnetic Resonance Force Microscopy on a Thin Permalloy Film

T. Mewes – University of Alabama

et al.

Citation of published version:

Nazaretski, E., et al. (2007): Ferromagnetic Resonance Force Microscopy on a Thin Permalloy Film, *Applied Physics Letters*, 90(23). https://doi.org/10.1063/1.2747171

Ferromagnetic resonance force microscopy on a thin permalloy film

E. Nazaretski, I. Martin, R. Movshovich, D. V. Pelekhov, P. C. Hammel, M. Zalalutdinov, J. W. Baldwin, B. Houston, and T. Mewes

Citation: Appl. Phys. Lett. **90**, 234105 (2007); doi: 10.1063/1.2747171

View online: https://doi.org/10.1063/1.2747171

View Table of Contents: http://aip.scitation.org/toc/apl/90/23

Published by the American Institute of Physics

Ferromagnetic resonance force microscopy on a thin permalloy film

E. Nazaretski,[a] I. Martin, and R. Movshovich
Los Alamos National Laboratory, Los Alamos, New Mexico 87545

D. V. Pelekhov and P. C. Hammel
Department of Physics, Ohio State University, Columbus, Ohio 43210

M. Zalalutdinov
SFA Inc., Crofton, Maryland 21114

J. W. Baldwin and B. Houston
Naval Research Laboratory, Washington, D.C. 20375

T. Mewes
Department of Physics and Astronomy, University of Alabama, Tuscaloosa, Alabama 35487

(Received 17 November 2006; accepted 11 May 2007; published online 7 June 2007)

Ferromagnetic resonance force microscopy (FMRFM) offers a means of performing local ferromagnetic resonance. The authors have studied the evolution of the FMRFM force spectra in a continuous 50 nm thick permalloy film as a function of probe-film distance and performed numerical simulations of the intensity of the FMRFM probe-film interaction force, accounting for the presence of the localized strongly nonuniform magnetic field of the FMRFM probe magnet. Excellent agreement between the experimental data and the simulation results provides insight into the mechanism of FMR mode excitation in a FMRFM experiment. © *2007 American Institute of Physics*. [DOI: 10.1063/1.2747171]

Magnetic resonance force microscopy (MRFM) offers a very high sensitivity approach to detection of magnetic resonance and has demonstrated three dimensional imaging with excellent spatial resolution. Proposed by Sidles,[1] it has been used for the detection of electron spin resonance,[2] nuclear magnetic resonance;[3] recently Rugar *et al.* reported detection of a force signal originating from a single electron spin,[4] emphatically demonstrating MRFM sensitivity. Incorporating basic elements of magnetic resonance imaging (MRI), MRFM can provide much higher spatial resolution than conventional MRI. Electron spin density images with micrometer scale resolution in an arbitrarily shaped sample can be deconvolved from MRFM spatial force maps.[5] MRFM image deconvolution requires a thorough understanding of the underlying interaction between the MRFM probe and the object imaged. This deconvolution process, analyzed for the case of noninteracting spins in a paramagnetic sample is given in Ref. 6. Recently, ferromagnetic resonance (FMR) has been detected by MRFM in yttrium iron garnet (YIG) bar,[7] YIG dot,[8,9] YIG film,[10] and permalloy dots.[11] The role of the probe magnet in FMRFM is dual: it both perturbs the FMR modes and detects the force signal. However, in Refs. [7–9] the FMR modes were only weakly modified by the tip field.

In this letter we focus on the regime when the effect of the tip is nonperturbative: the field inhomogeneity due to the tip field strongly modifies the resonance modes as well as leads to the formation of the *local* resonance under the tip. We report FMRFM spectra from a continuous, 50 nm thick permalloy film, performed with a cantilever with a nearly spherical micron-size magnetic tip. We report the evolution of the FMRFM spectra as a function of the tip-sample spacing and propose a model which describes the observed behavior.

The cantilever is mounted on top of a double scanning stage, comprised of a three dimensional attocube scanner[12] for coarse scanning and a piezotube for fine scanning. The optical feedback control of the attocube allows to position and move the cantilever stage with an accuracy better than 250 nm. The microwave power is used to manipulate the sample magnetization and is generated by the Giga-tronics 12000A synthesizer at a frequency $\omega_{rf}/2\pi=9.55$ GHz, 79 mW of power, and amplitude modulated with a modulation depth of 70%. It is fed into a strip line resonator with the broad resonant characteristics and allows to record FMRFM spectra in the frequency range between 9 and 11.5 GHz. A more detailed description of the microscope can be found elsewhere.[13] Contrary to MRFM experiments where the state-of-the-art ultrasensitive cantilevers are required to achieve high sensitivity[4] in FMRFM due to much stronger signals commercially available cantilevers can be used. We use a silicon nitride cantilever with a fundamental resonant frequency $\omega_c/2\pi\approx 8.06$ kHz and a spring constant $k\sim 10$ mN/m. The magnetic tip is a 2.4 μm diameter spherical $Nd_2Fe_{14}B$ particle[14] shown in the inset to Fig. 2. We removed the original tip of the cantilever by focused ion milling and manually glued the magnetic sphere to the cantilever with Stycast 1266 epoxy in the presence of an aligning magnetic field of a few kiloersteds. The 50 nm thick permalloy film was deposited on a 20 nm thick Ti adhesion layer on a 100 μm thick silicon wafer. The permalloy was capped with a protective of 20 nm Ti layer. An approximately 2×2 mm^2 sample was glued to the strip line resonator and the film plane was oriented perpendicular to the direction of the external magnetic field H_{ext}. In Fig. 1, we show the *magnitude* of the FMRFM spectra recorded as a function of the probe-sample distance at a constant temperature

[a]Electronic mail: evgnaz@lanl.gov

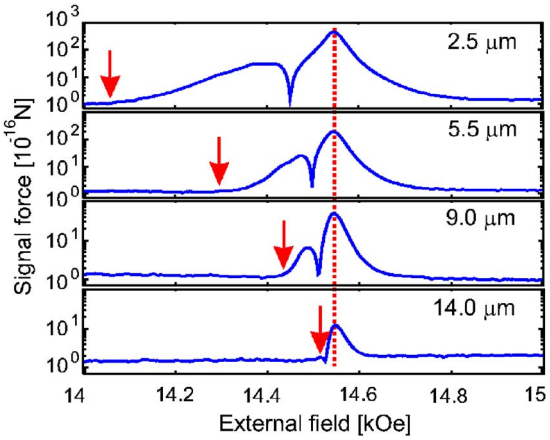

FIG. 1. (Color online) *Magnitude* of the FMRFM signals as a function of the probe-film spacing. The dotted line indicates the position of the main resonance peak, independent of the probe-film distance. The arrows mark the onset of the lower field resonance feature. The sharp dip in the magnitude spectrum indicates the change of sign of the force acting on the cantilever and approximately separates local resonance (in the region of the positive tip field) from the main resonance (region of the weak negative tip field). Experimental parameters: $\omega_{rf}/2\pi=9.55$ GHz, $T=11$ K.

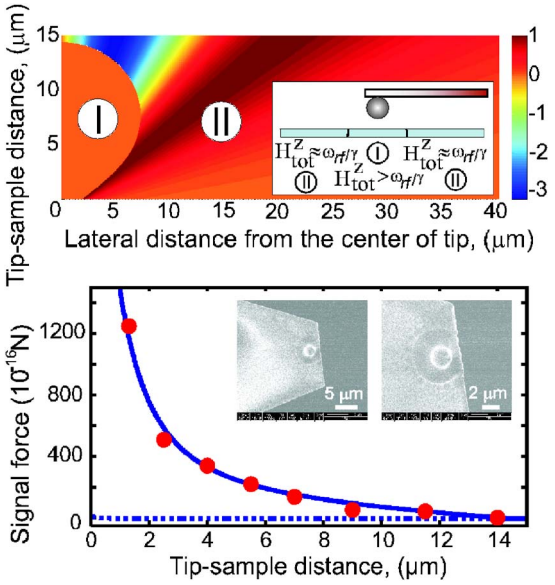

FIG. 2. (Color online) Upper panel: force map of the FMRFM probe-film interaction. The force acting on a cantilever due to an elementary ring-shaped area is calculated as a function of radius of the ring and the cantilever-film spacing. The force map is normalized to a maximum positive force value at each probe-film distance. Force contribution from region I of the sample is set to zero because the fundamental resonant mode which occurs at H_{res} does not significantly penetrate into region I, where $H_{tot}^{z}>\omega_{rf}/\gamma$. The inset shows schematically the probe-sample arrangement and two regions of the sample contributing to the FMRFM signal. Lower panel: integrated probe-film interaction force as a function of the cantilever-film spacing for the main resonance peak at $H_{ext}\sim 14.54$ kOe. The solid symbols represent experimental points and the solid line is the result of calculations based on the exclusion of region I. The dashed line shows the force if region I was included in integration. In this case there is no force exerted by a uniformly magnetized infinite film on a spherical probe tip. Two insets show scanning electron microscopy micrographs of the cantilever tip.

$T=11.000\pm0.005$ K. Each spectrum displays two distinctive features: the main resonance signal, which occurs at approximately $H_{ext}\approx 14.54$ kOe, and the secondary resonance structure at lower fields. The structure of the FMRFM signal is reminiscent of those observed in permalloy microstructures.[11] The intensities of both features decrease as the probe magnet is moved away from the surface of the sample. It is important to note that retraction of the probe does not change the position of the main resonance peak significantly, and at the same time the width of the secondary feature changes substantially. The quality factor Q of the cantilever decreases from $\sim 11\,000$ to ~ 6000 as the probe approaches the sample. The change in Q is due to tip-sample interactions (other than magnetic resonance) and is consistent with previous reports.[15–17] We measured Q by two methods (ring-down technique and swept frequency through resonance) at each probe-film spacing and subsequently calculated the magnitude of the force signal acting on the cantilever, Fig. 1.

In general, the force $\mathbf{F}$ detected in a MRFM experiment is a convolution of $\delta\mathbf{m}(\mathbf{r},t)$ (the change in sample magnetization due to rf manipulation) with the field gradient $\nabla\mathbf{H}_{tip}(\mathbf{r})$ of the magnetic tip. The force is given by the following volume integral: $\mathbf{F}=\int_{V_s}(\delta\mathbf{m}(\mathbf{r},t)\cdot\nabla)\mathbf{H}_{tip}(\mathbf{r})d\mathbf{r}$. In our experiments, the spherical shape of the probe magnet allows analytical calculation of its magnetic field profile $\mathbf{H}_{tip}(\mathbf{r})$ (Ref. 18) and is used to provide precise knowledge of the magnetization term $\delta\mathbf{m}(\mathbf{r},t)$ needed to interpret FMRFM spectra correctly.

The total magnetic field inside the sample is $\mathbf{H}_{tot}=\mathbf{H}_{ext}+\mathbf{H}_{tip}+\mathbf{H}_{d}$, where $\mathbf{H}_{ext}$ is a uniform external magnetic field, $\mathbf{H}_{tip}$ is a nonuniform magnetic field of the probe magnet, and $\mathbf{H}_{d}$ is the demagnetizing field. The exact spatial profile of $\mathbf{H}_{tot}$ depends on the total magnetic moment of the probe magnet, the probe-film spacing, and the relative orientation of $\mathbf{H}_{ext}$ with respect to the orientation of probe magnet magnetization (in our case they are parallel). The well defined shape of the magnetic tip allows us to schematically divide the sample into two regions according to the magnitude of the $\hat{\mathbf{z}}$ component of the total magnetic field H_{tot}^{z}. The first, region I, is a circular region directly under the magnetic tip where its field is significant and positive. The area of this region is determined by the distance between the center of the probe tip and the sample. In region II the field of the probe is much weaker and negative and its area encompasses the remaining sample area of $\sim 2\times 2$ mm^2. The schematics of two regions is shown in the inset to Fig. 2.

For a conventional FMR experiment the expected resonance field for the uniform FMR mode is $H_{res}^{u}=\omega_{rf}/\gamma+4\pi M_s$, where we neglect the anisotropy contribution,.[17,19] For our experimental parameters $\gamma/2\pi=2.89\pm0.05$ GHz/kOe (Ref. 17) and $\omega_{rf}/2\pi=9.55$ GHz, we obtain the value of $H_{res}^{u}=14.6$ kOe, which agrees within the error with the observed resonance field for the main peak (dotted line in Fig. 1); we thereby attribute it to the resonance originating from region II of the sample and representing its large area. The main resonance peak in Fig. 1 can be understood as the fundamental FMR mode observed in conventional FMR experiments,[20,21] modified by the tip field. Analytical derivation of the exact profile of such a modified mode is difficult, so we have performed micromagnetic simulations based on the numerical solution of the Landau-Lifshitz-Gilbert equation.[22] For simulation we used a damping constant $\alpha=0.01$, an exchange constant $A=1.4\times10^{-6}$ erg cm^{-1}, and values of $4\pi M_s=13.2$ kG for the probe magnet and $4\pi M_s=11.3$ kG for the permalloy film were measured independently by the superconducting quantum interface device magnetometry.[23] Simulations indicate that the FMR mode

excited in region II of the sample at the resonant field H_{res} does not penetrate significantly into spatial region I, where $H_{tot}^{z} > \omega_{rf}/\gamma$. We will present details of the analysis elsewhere.[24]

We assign the lower field feature in the FMRFM spectra shown in Fig. 1 to the resonance contributions originating from the *localized* FMR excitations spatially confined approximately to region I of the sample. In this region, the resonance occurs at lower values of H_{ext} than that of the main peak (Fig. 1, dotted line). The frequency shift of localized FMR is determined by two factors: (1) the strength of the tip field H_{tip} at the sample surface and (2) the effect of mode confinement to the spatial region I with characteristic dimensions defined by the tip-sample distance, which further increases the local mode frequency relative to the bulk resonance by a value $\Delta\omega_{conf}(r')$. Both effects cause the local resonance to occur at the external field value that is *lower* than that of the bulk resonance by the amount $\Delta H_{ext} \approx -H_{tip}(r') - \Delta\omega_{conf}(r')/\gamma$. From numerical simulations,[24] for a confinement within a disk of radius $r' \sim 10\ \mu$m, $\Delta\omega_{conf}(r')/\gamma \approx 30$ Oe, which combined with the estimated value of $H_{tip}(r') \approx 20$ Oe, results in a total shift consistent with experimental findings. Both the tip field H_{tip} and $\Delta\omega_{conf}(r')$ decrease as the probe magnet is retracted away from the film surface, and local modes merge into the main resonance (Fig. 1, dotted line).

The non-Lorentzian and broad shape of the signal possibly indicates the presence of multiple modes contributing to the resonance. While numerical simulations are required to determine the possibility of such modes, in particular, geometry/materials, we believe that their appearance is generic in thin-film soft magnets and is induced by the local field inhomogeneity. We will present the detailed theoretical analysis elsewhere.[24]

The normalized FMRFM spatial force map obtained from the uniform FMR mode modified by the tip field is shown in Fig. 2. The semicircular region of the plot where the tip-sample interaction force is set to zero corresponds to region I. In the lower panel of Fig. 2 we show the intensity of the main resonance signal as a function of the tip-sample distance and compare simulations with the experiment.

In conclusion, we conducted FMRFM experiments in a thin permalloy film. We performed quantitative analysis of the force exerted by the fundamental mode and observed locally excited FMR. We conducted simulations and determined two distinctive regions of the sample contributing to the FMRFM spectra. We find clear evidence for local modification of the FMR mode structure by the probe tip, providing insight into the interaction of the probe tip with ferromagnetic samples in FMRFM.

The work performed at Los Alamos National Laboratory was supported by the U.S. Department of Energy, Center for Integrated Nanotechnologies, Contract No. W-7405-ENG-36 at Los Alamos National Laboratory and Contract No. DE-AC04-94AL85000 at Sandia National Laboratories. The work at Ohio State University was supported by the U.S. Department of Energy through Grant No. DE-FG02-03ER46054. The work at Naval Research Laboratory (NRL) was supported by the Office of Naval Research through the Institute for Nanoscience at NRL.

[1] J. A. Sidles, Appl. Phys. Lett. **58**, 2854 (1991).
[2] D. Rugar, C. S. Yannoni, and J. A. Sidles, Nature (London) **360**, 563 (1993).
[3] D. Rugar, O. Züger, S. Hoen, C. S. Yannoni, H. M. Vieth, and R. D. Kendrick, Science **264**, 1560 (1994).
[4] D. Rugar, R. Budakian, H. J. Mamin, and W. Chui, Nature (London) **430**, 329 (2004).
[5] O. Züger and D. Rugar, Appl. Phys. Lett. **63**, 2496 (1993).
[6] A. Suter, D. V. Pelekhov, M. L. Roukes, and P. C. Hammel, J. Magn. Reson. **154**, 210 (2002).
[7] Z. Zhang, P. C. Hammel, and P. E. Wigen, Appl. Phys. Lett. **68**, 2005 (1996).
[8] V. V. Naletov, V. Charbois, O. Klein, and C. Fermon, Appl. Phys. Lett. **83**, 3132 (2003).
[9] V. Charbois, V. V. Naletov, J. Ben Youssef, and O. Klein, Appl. Phys. Lett. **80**, 4795 (2002).
[10] R. Urban, A. Putilin, P. E. Wigen, S.-H. Liou, M. C. Cross, P. C. Hammel, and M. L. Roukes, Phys. Rev. B **73**, 212410 (2006).
[11] T. Mewes, J. Kim, D. V. Pelekhov, G. N. Kakazei, P. E. Wigen, S. Batra, and P. C. Hammel, Phys. Rev. B **74**, 144424 (2006).
[12] www.attocube.com, models ANPx(z) 100/LIN
[13] E. Nazaretski, T. Mewes, D. Pelekhov, P. C. Hammel, and R. Movshovich, AIP Conf. Proc. **850**, 1641 (2006).
[14] http://www.magnequench.com/assets/download/MQP-S-11-9.pdf
[15] I. Dorofeyev, H. Fuchs, G. Wenning, and B. Gotsmann, Phys. Rev. Lett. **83**, 2402 (1999).
[16] B. C. Stipe, H. J. Mamin, C. S. Yannoni, T. D. Stowe, T. W. Kenny, and D. Rugar, Phys. Rev. Lett. **87**, 277602 (2001).
[17] E. Nazaretski, J. D. Thompson, M. Zalalutdinov, J. W. Baldwin, B. Houston, T. Mewes, D. V. Pelekhov, P. Wigen, P. C. Hammel, and R. Movshovich, J. Appl. Phys. **101**, 074905 (2007).
[18] J. D. Jackson, *Classical Electrodynamics* 3rd ed. (Wiley, New York, 1999), p. 194.
[19] Z. Frait, Physica B & C **86-88**, 1241 (1977).
[20] C. Herring and C. Kittel, Phys. Rev. **81**, 869 (1951).
[21] M. Sparks, B. R. Tittmann, J. E. Mee, and C. Newkirk, J. Appl. Phys. **40**, 1518 (1969).
[22] T. L. Gilbert, Phys. Rev. **100**, 1243 (1955); L. D. Landau, E. M. Lifshitz, and L. P. Pitaevski, *Statistical Physics*, 3rd ed. (Butterworth-Heinemann, Oxford, England, 1980) Vol. 9, Part 2, Chap. 7, p. 284.
[23] E. Nazaretski, J. D. Thompson, D. V. Pelekhov, T. Mewes, P. E. Wigen, J. Kim, M. Zalalutdinov, J. W. Baldwin, B. Houston, P. C. Hammel, and R. Movshovich, J. Magn. Magn. Mater. **310**, 941(E) (2006).
[24] D. V. Pelekhov (to be published).